

Single-forward-jet tagging and central-jet vetoing to identify the leptonic WW decay mode of a heavy Higgs boson

V. Barger and Kingman Cheung

Department of Physics, University of Wisconsin, Madison, Wisconsin 53706

T. Han

Fermi National Accelerator Laboratory, P. O. Box 500, Batavia, Illinois 60510

D. Zeppenfeld

Department of Physics, University of Wisconsin, Madison, Wisconsin 53706

(Received 30 May 1991)

We study the extraction of the heavy-Higgs-boson signal $H \rightarrow W^+W^- \rightarrow \bar{\ell}\nu, \ell\bar{\nu}$ ($\ell = e$ or μ) from the standard-model background at hadron supercolliders. By tagging a single forward jet with energy $E_j > 3$ TeV and pseudorapidity $3 < |\eta_j| < 5$ and by vetoing central jets of transverse momenta $p_{Tj} > 60$ GeV in the pseudorapidity range $0 < |\eta_j| < 3$, the QCD WWj and $t\bar{t}j \rightarrow WWb\bar{b}j$ backgrounds are suppressed. For $m_H = 1$ TeV there are about 46 signal events from electroweak-vector-boson scattering (of which 36 events are of Higgs-boson origin) at the Superconducting Super Collider (SSC) for an integrated luminosity of 10 fb^{-1} and 10 other events from the WWj and $t\bar{t}j$ backgrounds for $m_t = 140$ GeV. The experimental separation of the vector-boson-scattering subprocess is thereby possible. At the CERN Large Hadron Collider, with an $E_j > 2$ TeV jet energy cut, all cross sections are about a factor of 10 below the SSC values.

I. INTRODUCTION

The nature of the electroweak-symmetry-breaking mechanism is a fundamental question in contemporary high-energy physics. Experimental searches for the neutral Higgs boson (H), the relic of electroweak symmetry breaking in the standard model (SM), presents a major challenge [1]. The mass of the Higgs boson is undetermined in the SM so one must be prepared to search over a mass range extending up to the unitarity bound of order $m_H = 1$ TeV and possibly beyond for strong VV ($V = W, Z$) scattering effects [2–4] if a resonant scalar state is not found at lower mass.

If the Higgs boson has a mass $m_H > M_Z$, then the CERN Large Hadron Collider (LHC) and Superconducting Super Collider (SSC) will be the first generation of machines capable of finding it. For m_H in the range $2M_Z < m_H < 800$ GeV, the decay mode of principal interest is $H \rightarrow ZZ \rightarrow \ell\bar{\ell}, \ell\bar{\ell}$ ($\ell = e$ or μ), since these modes provide especially distinctive signatures. However, the four-charged-lepton mode has a rather small rate, since the $H \rightarrow ZZ \rightarrow 4\ell$ branching fraction is only 0.14%. The mode $H \rightarrow W^+W^- \rightarrow \ell\nu, jj$ with one W decaying into jets, has been intensively studied as a possible alternative signal [3] since this mode has a branching fraction of 20%. Unfortunately the SM backgrounds from QCD Wjj production [5] (with a dijet invariant mass close to M_W) and from top-quark pairs [6–8] are daunting. Extensive studies have found a signal-to-background ratio smaller than unity [9].

The double leptonic mode $H \rightarrow W^+W^- \rightarrow \bar{\ell}\nu\ell\bar{\nu}$ has a

branching fraction of 3.1% and is free from the QCD Wjj background. The major disadvantage of this channel is that the Higgs-boson mass cannot be precisely reconstructed, because two neutrinos are missing. However, this is not such an important consideration since a heavy Higgs boson has a very broad resonance structure. In addition, one would like to measure the $H \rightarrow W^+W^-$ channel not only to find the Higgs boson, but also to study its properties, such as determining the relative coupling strength of the Higgs boson to ZZ and to WW .

In this paper, we study the feasibility of a heavy-Higgs-boson search in the W^+W^- leptonic channel. The SM background from W^+W^- production in association with QCD jets [10, 11] can be eliminated by tagging a single high-energy jet in the forward region. A much larger background arises from $t\bar{t}j \rightarrow W^+W^-b\bar{b}j$. The Collider Detector at Fermilab (CDF) bound [12] $m_t > M_W$ implies that the $t \rightarrow bW$ branching fraction in the SM is essentially 100%. At the outset this background is several orders of magnitude larger than the Higgs-boson signal but it can be reduced to the level of the signal by tagging a single energetic forward jet. In addition, there is considerable jet activity in the central region due to b quarks from t decays. By a central-jet veto the $t\bar{t}j$ background can be suppressed by another order of magnitude. After imposing appropriate jet-selection criteria, there are about 46 electroweak signal events (of which 36 events are of $m_H = 1$ TeV origin) and 10 WWj and $t\bar{t}j$ background events at the SSC ($\sqrt{s} = 40$ TeV) for an integrated luminosity of 10 fb^{-1} . At the LHC ($\sqrt{s} = 16$ TeV) the corresponding numbers are about 5 electroweak signal events and 1 background event per 10 fb^{-1} .

The paper is organized as follows. In Section II we describe the calculations for the signal and the backgrounds. The implementation of kinematical jet cuts to enhance the signal over the background is discussed in Section III. In Section IV we give an overview of the leptonic observables after forward-jet tagging and central-jet vetoing and we discuss to what extent they may serve to suppress the electroweak background from transverse W -boson production. Section V gives a summary of our results. The calculation of the $qq \rightarrow qqWW$ electroweak subprocess is described in the Appendix.

II. CALCULATIONS OF PROCESSES PRODUCING $W^+W^- + \text{JETS}$

The Higgs boson can be produced at hadron supercolliders via the subprocesses

$$gg \rightarrow H \rightarrow W^+W^- , \quad (1)$$

and

$$qq \rightarrow qqH \rightarrow qqW^+W^- . \quad (2)$$

Although for a heavy top quark the $gg \rightarrow H \rightarrow W^+W^-$ cross section [13] is dominant for m_H up to ~ 1 TeV, this contribution cannot be separated from the large backgrounds from $gg \rightarrow t\bar{t} \rightarrow W^+W^-b\bar{b}$ and $q\bar{q} \rightarrow W^+W^-$ production. Hence, jet-inclusive searches for the Higgs signal are not feasible in the W^+W^- channel, unlike the situation for $H \rightarrow ZZ$.

On the other hand, the $qq \rightarrow qqH$ subprocess provides an additional handle for identification via the final-state quarks emitted at high energies and forward angles. The primary backgrounds in this case are

$$gg \rightarrow t\bar{t} , \quad (3a)$$

$$gg \rightarrow t\bar{t}g , \quad (3b)$$

$$qq \rightarrow t\bar{t}q , \quad (3c)$$

$$q\bar{q} \rightarrow t\bar{t}g , \quad (3d)$$

and

$$qq \rightarrow W^+W^-q , \quad (4a)$$

$$q\bar{q} \rightarrow W^+W^-g . \quad (4b)$$

We generally refer to the processes in Eq. (3) as $t\bar{t}j$ and to those in Eq. (4) as QCD WWj production, where j denotes a jet.

Jet tagging involves forward jets, and hence it is necessary to consider the backgrounds from $O(\alpha_s^3)$ $t\bar{t}j$ production rather than just $O(\alpha_s^2)$ $t\bar{t}$ production. An $O(\alpha_s^3)$ calculation [6, 7] is sufficient here because we will tag only one forward jet.

In the following we briefly present the basis of our signal and background calculations.

A. The electroweak processes $qq \rightarrow W^+W^-qq$

At $O(\alpha^4)$, electroweak processes contribute significantly to W^+W^- production in association with two quarks giving up to two visible jets. An incomplete set of Feynman graphs for these processes is shown in

Fig. 1. The major interest here is in the scattering of longitudinal vector bosons occurring in subprocesses such as the ones shown in Fig. 1(a) that include Higgs-boson resonance production. A full tree-level calculation of qqW^+W^- production must include the contributions to W^+W^- production in which the W bosons are radiated from external quark lines [see Figs. 1(b) and 1(c)]. These electroweak processes have been evaluated previously in Refs. [14] and [15]. We have independently performed a full calculation using the helicity-amplitude techniques of Ref. [16], and have checked against the calculation of Ref. [15] and find numerical agreement. In our calculation, we have also included the W -boson decays $W^+W^- \rightarrow \bar{\ell}\nu\ell\nu$, which was not done in previous analyses. For completeness our formulas are given in the Appendix. All our results are obtained with a Breit-Wigner form of the Higgs-boson propagator for the s -channel Higgs-boson exchange in Fig.1(a), taking an s -independent width Γ_H .

Many aspects of the electroweak calculation for $qq \rightarrow qqW^+W^-$ production are similar to that for $qq \rightarrow qqZZ$ and we refer the reader to our recent discussion of the latter [17]. We impose a $Q^2 > 5 \text{ GeV}^2$ cutoff on t -channel photon propagators and require a jet-jet separation cut $\Delta R_{jj} > 0.7$ for final-state partons throughout this paper.

The dominant electroweak contribution arises from the vector-boson fusion graphs of Fig.1(a). As seen by each of the two incoming protons this process resembles deep-inelastic lepton-proton scattering via W -boson exchange. This strongly suggests a scale choice in the structure functions which is related to the average virtuality of the incoming weak bosons. Thus we use $Q^2 = M_W^2$ as the scale in the calculation of the electroweak signal processes [18]. For the parton distribution functions we use

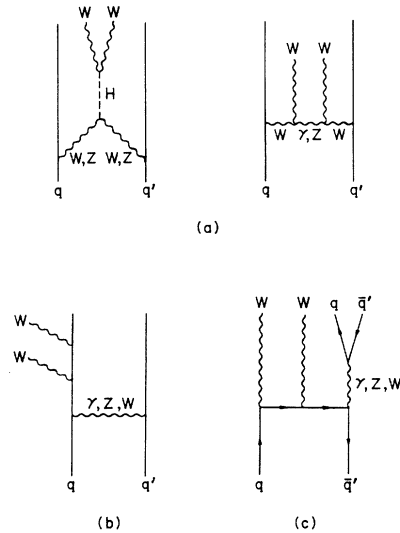


FIG. 1. Feynman diagrams for the electroweak processes $qq \rightarrow qqW^+W^-$. Representative diagrams are shown for (a) vector-boson fusion, (b) t -channel photon, Z , or W exchange, and (c) s -channel electroweak boson exchange.

the parametrization HMRS(B) of Harriman *et al.* [19].

The above scale argument is very important in connection with the vetoing of central jets. In determining the acceptance of the $qq \rightarrow qqWW$ signal we consider the second final-state parton (after forward-jet tagging) as a candidate for a central jet, but we need not take into account additional central parton radiation from higher-order QCD processes. In the lowest-order $qq \rightarrow qqWW$ process the two final-state quarks have an average transverse momentum $p_T \sim M_W$. Any additional radiation of partons with $p_T \gtrsim M_W/2$ occurs via hard processes which will be suppressed by additional powers of α_s and hence can be neglected.

We are principally interested in the electroweak contribution due to a heavy Higgs boson or other longitudinal weak-boson scattering mechanisms. In this context the electroweak production of transversely polarized W bosons may obscure the longitudinal W -boson scattering signal. Because of important interference effects between all the contributing Feynman graphs, the Higgs-boson contribution cannot be directly isolated. Rather, we use the SM perturbative calculation with a light Higgs boson ($m_H = 0.1$ TeV), where the W bosons are primarily transverse, to estimate contamination from transverse W -boson production; henceforth we call this the electroweak $qqWW$ background.

B. QCD W^+W^-j background

The tree-level results for $W^+W^- + 1$ jet production [10, 11] are the basis for our estimates of the QCD background to single jet tagging. Gluon emission from a quark leg leads to both infrared and collinear singularities in the tree-level cross-section formulas. These singularities can be avoided by implementing experimental acceptances in the calculation. As discussed in Ref. [17], we impose a cut on the jet energy $E_{j\min}$, as measured in the lab frame, in order to regularize the soft divergencies, and the collinear singularities are eliminated by requiring the jet to have a pseudorapidity $|\eta_j| < |\eta_j|_{\max} = 5$. We choose a scale $Q^2 = M_W^2$ in both the strong coupling constant α_s and in the structure functions for all our QCD WWj background calculations.

In our analysis we do not consider $W^+W^- +$ jet production via pentagon, box, and triangle loops because no full calculation of these $O(\alpha_s^3)$ processes exists. However, we expect these contributions to be smaller than the tree-level contributions since the lowest-order loop result for the $gg \rightarrow W^+W^-$ cross section is somewhat smaller than the tree-level $q\bar{q} \rightarrow W^+W^-$ cross section [13]. Furthermore, our jet-tagging procedure will effectively eliminate the tree-level QCD contributions to W^+W^-j final states, and we expect equally effective suppression of the loop contributions with jets.

C. $t\bar{t}j$ Background

We wish to calculate the $t\bar{t}$ background in such a way that it generates the dynamical distributions of the $O(\alpha_s^3)$ processes listed in Eqs. (3b)-(3d). The relevant cross-

section formulas are given in Ref. [6]. We also want to reproduce the full one-loop corrected $t\bar{t}$ production cross section [7] when the extra jet becomes soft. The truncated shower (TS) approximation [20] incorporates the above features. The tree-level $t\bar{t} + 1$ jet differential cross section $d\sigma(t\bar{t}j)_{\text{TL}}$ is replaced by

$$d\sigma(t\bar{t}j)_{\text{TS}} = d\sigma(t\bar{t}j)_{\text{TL}}(1 - e^{-cp_{Tj}^2}), \quad (5)$$

with the constant c properly chosen to correctly reproduce the full $O(\alpha_s^3)$ total cross section. As $p_{Tj} \rightarrow 0$ the final factor in Eq. (5) acts as a regulator. For both SSC and LHC energies, we find that

$$c = \left(\frac{1}{20 \text{ GeV}} \right)^2$$

gives the desired result for $m_t = 140$ GeV. In effect our calculations are very insensitive to this regulator: our final jet acceptance criteria of $E_j(\text{tag}) > 3$ TeV, $3 < |\eta_j(\text{tag})| < 5$ always give $|p_{Tj}| > 40$ GeV and then the regulator in Eq. (5) is nearly unity. We choose the transverse energy squared $m_t^2 + p_T^2$ of the top quark as the Q^2 scale in the structure functions and in α_s .

In calculating the distributions of the final-state particles in $t \rightarrow Wb \rightarrow \ell\nu b$ decays, we include full spin correlations in the decay matrix elements, but we neglect the polarization effects of the parent top quark which are known to be small [21].

III. EVENT-SELECTION CRITERIA

We have recently shown that single jet tagging provides an effective means of suppressing the QCD backgrounds to the $qq \rightarrow qqZZ$ signal from heavy-Higgs-boson production [17]. In a completely analogous fashion we expect to be able to suppress the QCD WWj background to the Higgs-boson signal in $qq \rightarrow qqW^+W^-$. A more serious concern is the $t\bar{t}j \rightarrow W^+W^-b\bar{b}j$ background which is initially 2–3 orders of magnitude larger than the signal. We will employ jet tagging to help suppress this background as well. In the study of strong vector-boson scattering signals in the $qq \rightarrow qqW^+W^+$ process [4], it was found that a veto of events in which there was a hard central jet was effective in suppressing the $t\bar{t}W^+$ background. In this vein we shall use jet vetoing in the central region [4, 22] together with forward-jet tagging to achieve the necessary suppression of the background.

Throughout this paper, we are studying the purely leptonic decay mode $H \rightarrow W^+W^- \rightarrow \ell\nu\ell\bar{\nu}$ ($\ell = e, \mu$). We incorporate the full matrix elements of the W decays in the calculations of both signal and backgrounds. In order to simulate the detector coverage for the leptons and to enhance the signal-to-background ratio, we will, unless stated otherwise, implement the following lepton acceptance cuts on the transverse momentum and rapidity,

$$p_{T\ell} > 100 \text{ GeV}, \quad |y_\ell| < 2, \quad (6)$$

and include the branching fraction of W leptonic decays in the results.

A. Single-forward-jet tagging

Following the jet-tagging criteria of Ref. [17] we start by requiring the presence of a single jet of energy and pseudorapidity

$$E_j > 1 \text{ TeV} \quad \text{and} \quad |\eta_j| < 5. \quad (7)$$

When more than one jet satisfies this condition we define the tag jet to be the most energetic one. Figure 2 gives the distribution $d^2\sigma/dE_j d|\eta_j|$ at the SSC for the $m_H = 1$ TeV heavy-Higgs-boson signal, the $m_H = 0.1$ TeV case, the QCD WWj background, and the background due

to $t\bar{t}j$ production with $t \rightarrow Wb$ decay for a top-quark mass of $m_t = 140$ GeV. Notice that both backgrounds are concentrated at low jet energies while the signal is more or less uniform in jet energy. Moreover, the signal is concentrated at large pseudorapidities ($|\eta_j| > 2$). Even at the edge of phase space, when $|\eta_j| \approx 5$ and $E_j \approx 1$ TeV, the regularization factor in Eq. (5) is only about 0.4 and thus the TS approach does not significantly reduce the perturbative $t\bar{t}j$ cross section.

The different features of the tagged jet in the signal versus the backgrounds are also evident in Fig. 3 where the pseudorapidity distributions $d\sigma/d|\eta_j|$ at the SSC are compared for minimum jet energies of 1 and 3 TeV. By

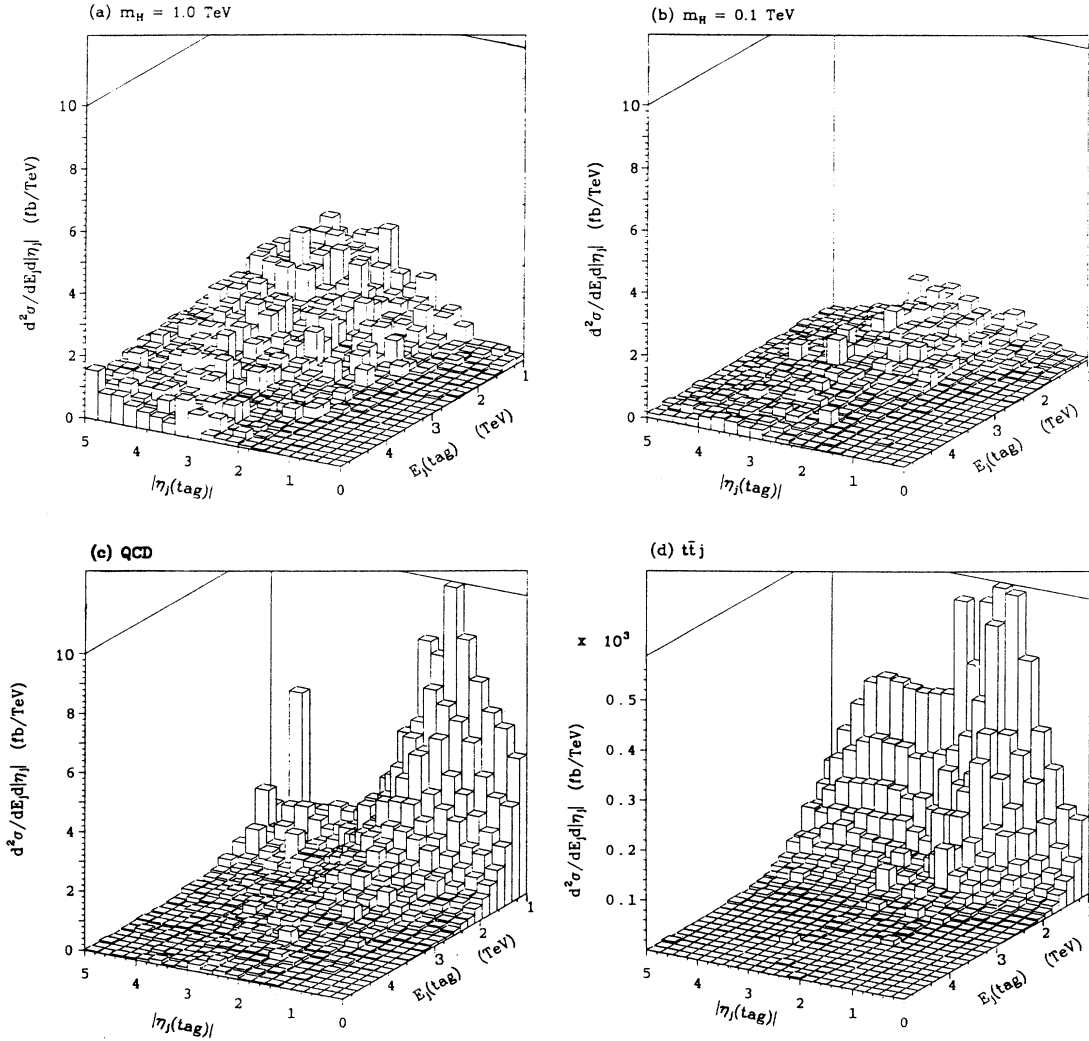


FIG. 2. $d^2\sigma/dE_j d|\eta_j|$ distributions of the tagged jet at the SSC from (a) the $m_H = 1$ TeV SM signal, (b) the SM electroweak $qqWW$ background ($m_H = 0.1$ TeV), (c) the QCD WWj background, and (d) the $t\bar{t}j$ background for $m_t = 140$ GeV. The jet and lepton acceptance are given in Eqs. (6) and (7).

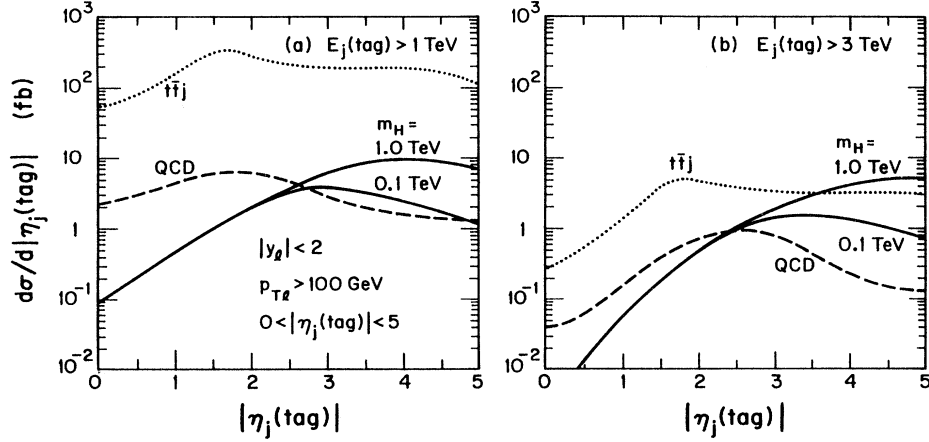


FIG. 3. Pseudorapidity distributions of the tagged jet for the $t\bar{t}j$, QCD WWj , and electroweak $qqWW$ ($m_H = 0.1$ TeV) backgrounds and the SM Higgs-boson signal for $m_H = 1$ TeV at the SSC for (a) $E_j > 1$ TeV, (b) $E_j > 3$ TeV. The lepton acceptance is given in Eq. (6).

using jet-tagging requirements of

$$E_j(\text{tag}) > 3 \text{ TeV} \quad \text{and} \quad 3 < |\eta_j(\text{tag})| < 5 \quad (8a)$$

at the SSC and

$$E_j(\text{tag}) > 2 \text{ TeV} \quad \text{and} \quad 3 < |\eta_j(\text{tag})| < 5 \quad (8b)$$

at the LHC, we succeed in reducing the backgrounds to the level of the $m_H = 1$ TeV signal.

B. Central jet vetoing

The major jet activity in the signal is at high pseudorapidities and low p_{Tj} . The radiation of additional jets in the central region is suppressed by factors of $\alpha_s(M_W^2) \ln[M_W^2/p_T^2(\text{cut})]$ where $p_T(\text{cut})$ refers to the

minimum transverse-momentum requirement of identified central jets. To avoid jets of minimum bias origin we choose $p_{Tj}(\text{cut}) = 60$ GeV. Then the bulk of the signal events contain no extra such central jets.

In contrast, the $t\bar{t}j$ background has copious jet activity in the central region due to the b jets from $t \rightarrow Wb$ decays. Only W bosons produced in the central region (e.g., $0 \leq |y_W| \lesssim 2$) can be identified via $W \rightarrow \ell\nu$, and then the b quarks from $t \rightarrow bW$ decay will also populate the central region. Thus a veto of events with extra jets in the central region satisfying

$$p_{Tj}(\text{veto}) > 60 \text{ GeV} \quad \text{and} \quad |\eta_j(\text{veto})| < 3 \quad (9)$$

will greatly suppress this background at little cost to the signal. The pseudorapidity distribution in Fig. 4 for the

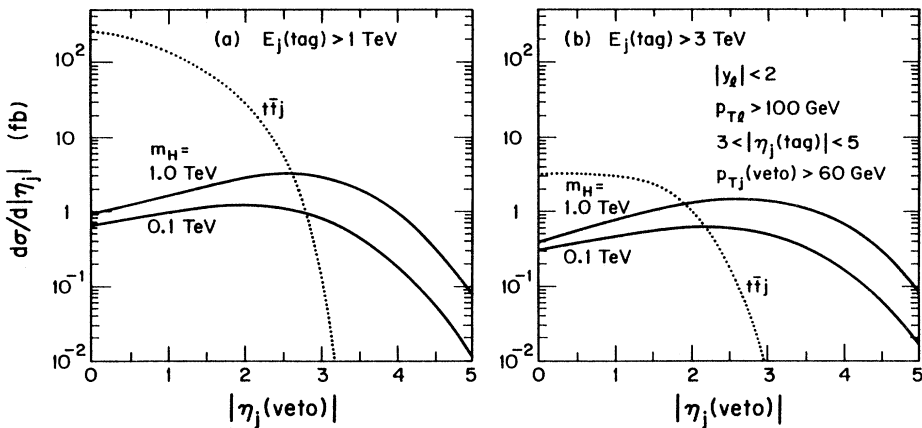


FIG. 4. Pseudorapidity distributions of the second jet (veto candidate) for the $t\bar{t}j$, electroweak $qqWW$ ($m_H = 0.1$ TeV) backgrounds and the SM Higgs-boson signal for $m_H = 1$ TeV at the SSC with a tagged jet requirement of (a) $E_j > 1$ TeV, (b) $E_j > 3$ TeV. The acceptance cuts as listed in (b) are imposed in both figures.

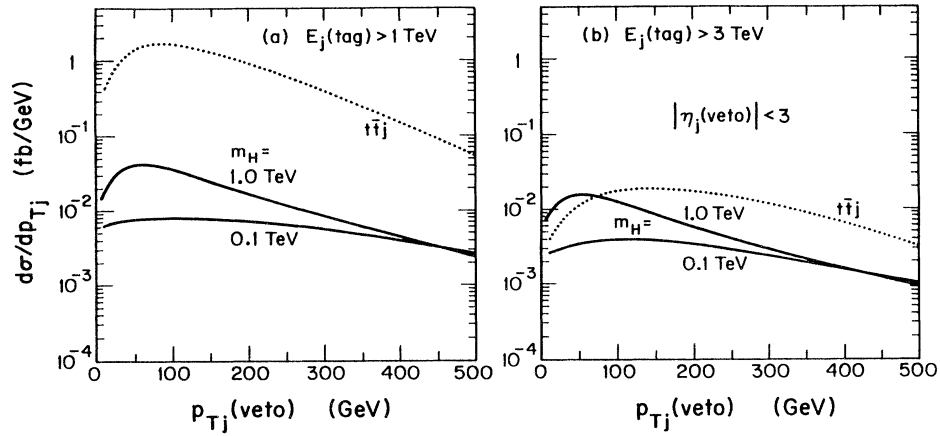


FIG. 5. Transverse momentum distributions of the second jet (veto candidate) with $|\eta_j(\text{veto})| < 3$ for the $t\bar{t}j$, electroweak $qqWW$ ($m_H = 0.1 \text{ TeV}$) backgrounds and the SM Higgs-boson signal for $m_H = 1 \text{ TeV}$ at the SSC. The tagged jet requirements are (a) $E_j > 1 \text{ TeV}$, (b) $E_j > 3 \text{ TeV}$. The acceptance criteria for leptons and jets are those of Eqs. (6) and (8a).

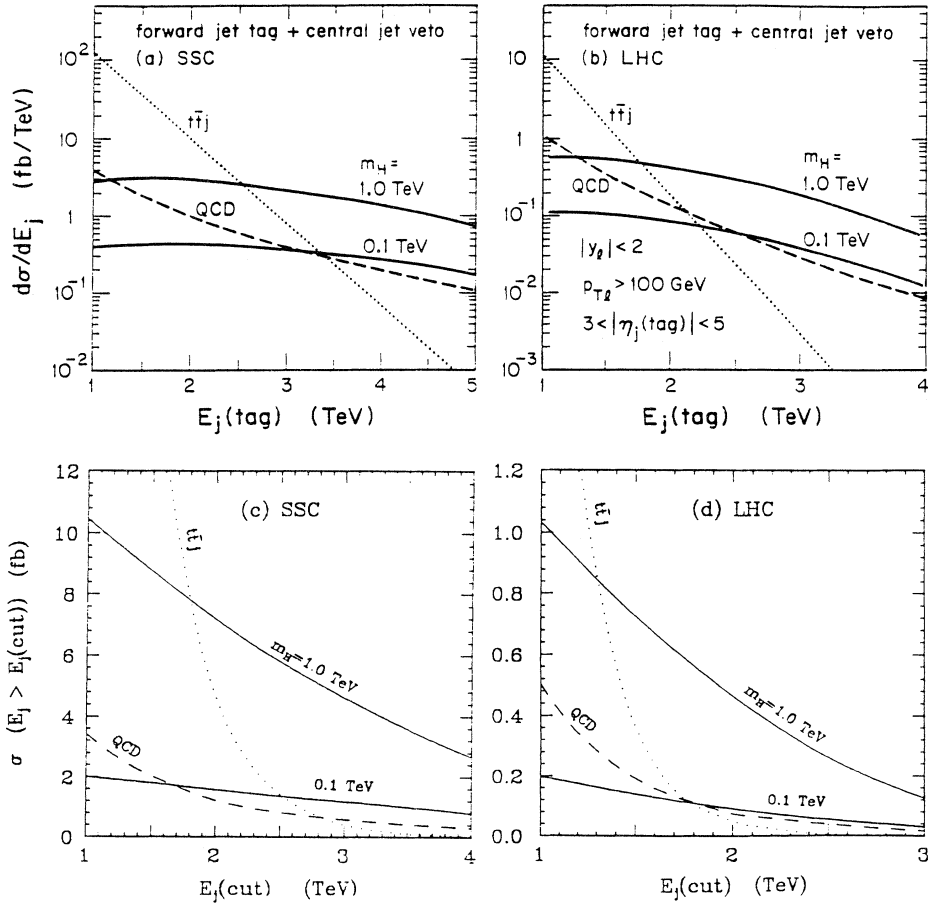


FIG. 6. Energy distribution (a) at the SSC and (b) at the LHC of the tagged jet with $3 < |\eta_j(\text{tag})| < 5$. The integrated cross section for the tagged jet energy $E_j(\text{tag})$ above a specified value $E_j(\text{cut})$ is given at (c) the SSC, and (d) the LHC. The SM Higgs-boson signals for $m_H = 1 \text{ TeV}$ are shown along with the $t\bar{t}j$, the QCD WWj , and the electroweak $qqWW$ ($m_H = 0.1 \text{ TeV}$) backgrounds. Acceptance criteria are given in Eqs. (6) and (9).

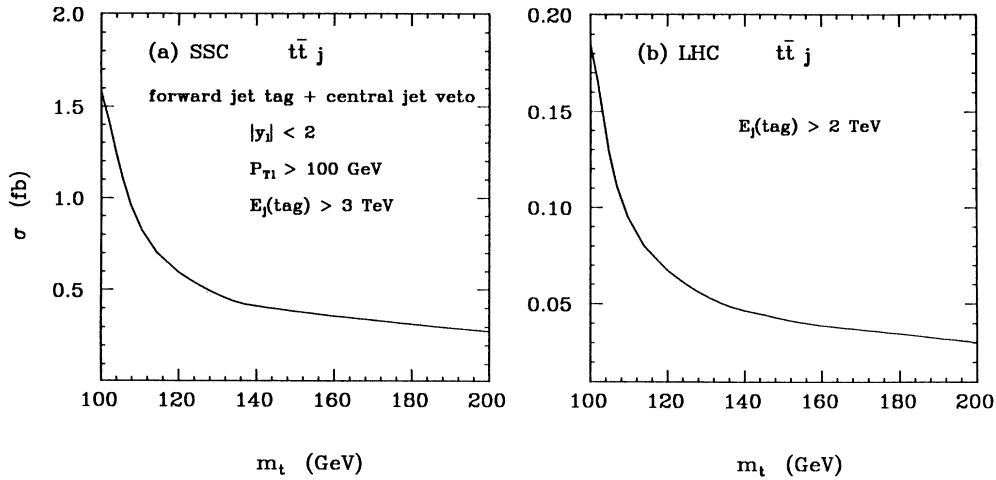


FIG. 7. Cross section for $t\bar{t}j$ events after forward-jet tagging and central-jet vetoing as a function of m_t (a) at the SSC and (b) at the LHC. Acceptance criteria are given in Eqs. (6), (8), and (9).

tor of 4 larger for $m_t = 100$ GeV than for $m_t = 140$ GeV. When m_t is close to M_W , the b quark from $t \rightarrow bW$ is relatively soft, so that the jet-veto requirement is less effective. However, even for $m_t = 100$ GeV our approach is successful in isolating the heavy-Higgs-boson signal. If we also require lepton isolation from hadrons, the $t\bar{t}j$ background for $m_t = 100$ GeV will be further reduced, with essentially no reduction of the heavy-Higgs-boson signal.

We show in Fig. 8 the transverse-momentum distribution of the tagged jet. The p_{Tj} distribution for the $m_H = 1$ TeV signal is relatively softer than for both the $m_H = 0.1$ TeV electroweak and the WWj QCD backgrounds, due to helicity suppression of transverse W production in the forward direction.

B. Lepton characteristics

Having succeeded in isolating the W^+W^- electroweak signal we proceed to a discussion of the characteristics of the resulting lepton distributions. Our purpose is to compare the features of the heavy-Higgs-boson signal with those expected from transverse W -pair production or the QCD backgrounds.

Figures 9 and 10 give rapidity and p_T distributions of the leptons. We see from these figures that our lepton acceptance cuts of Eq. (6) optimize the signal-to-background ratio, while retaining a sizable signal event rate. The shapes of the rapidity distributions are distinctly different for the electroweak and QCD processes, allowing a verification that the signal has in fact been

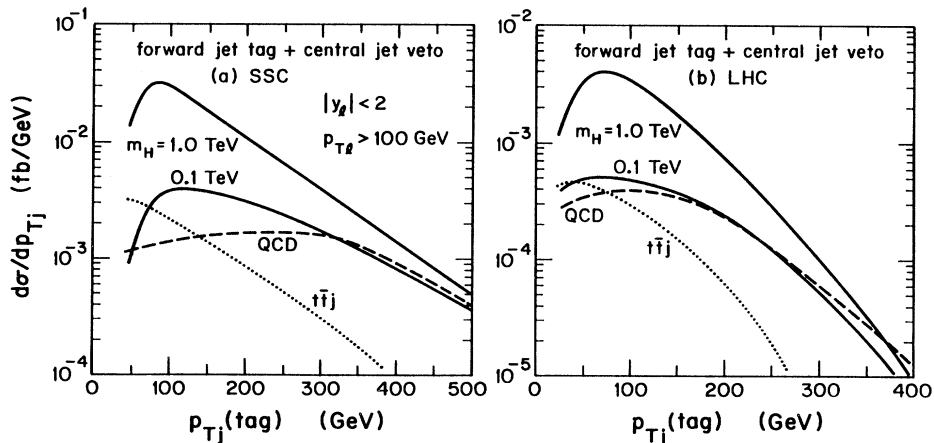


FIG. 8. Transverse-momentum distribution of the tagged jet in the Higgs-boson signal for $m_H = 1$ TeV, and the $t\bar{t}j$, the QCD WWj , and the electroweak $qqWW$ ($m_H = 0.1$ TeV) backgrounds at (a) the SSC and (b) the LHC. Jet and lepton acceptances are the same as in Fig. 7.

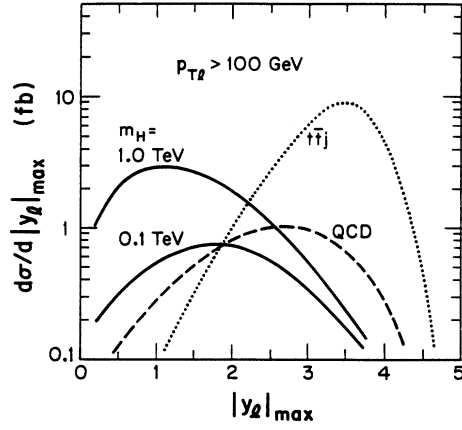


FIG. 9. Rapidity distribution $|y_\ell|_{\max}$ of the leptons with $p_{T\ell} > 100$ GeV for the $t\bar{t}j$, QCD WWj , and electroweak $qqWW$ ($m_H = 0.1$ TeV) backgrounds and the SM Higgs-boson signal for $m_H = 1$ TeV at the SSC. Acceptance criteria are given in Eqs. (8a) and (9).

isolated. In the p_T distributions the $m_H = 1$ TeV signal gives a much broader distribution than the transverse W or QCD backgrounds.

In all our considerations we have adopted $p_{T\ell} > 100$ GeV and $|y_\ell| < 2$ lepton cuts. It is appropriate to ask whether an improved signal-to-background ratio would be achieved by relaxing the lepton acceptance requirements. The results of relaxed $p_{T\ell}$ cuts are presented in part (a) of Table II. A smaller lepton p_T cut yields a substantially higher rate from $qq \rightarrow qqWW$ but this increase is mostly due to contributions from transverse W -boson production.

We may define the signal of a heavy Higgs boson with mass m_H as $S = [\sigma(m_H) - \sigma(m_H = 0.1 \text{ TeV})] \int \mathcal{L} dt$, with $\int \mathcal{L} dt$ the integrated luminosity, since the cross section with a light Higgs boson ($m_H \sim 0.1$ TeV) can be considered as a measure of electroweak contributions to $qqWW$ involving transverse W 's only. Correspondingly we may define a background as $B = [\sigma(m_H = 0.1 \text{ TeV}) + \sigma(t\bar{t}j) + \sigma(WWj)] \int \mathcal{L} dt$. Then S/\sqrt{B} is a measure of the significance of the signal. We give the significance values for various $p_{T\ell}$ cuts in Table II for $m_H = 1$ TeV, $m_t = 140$ GeV, and $\int \mathcal{L} dt = 10 \text{ fb}^{-1}$. The significance decreases as the $p_{T\ell}$ cut decreases. The 8σ significance for $p_{T\ell} > 100$ GeV should allow an unambiguous heavy-Higgs-boson discovery.

In the case of $W^+W^+ \rightarrow \bar{\ell}\nu\ell\nu$ events, distributions in the angle $\phi_{\ell\ell}$ between the leptons in the transverse plane and in the transverse-momentum difference,

$$\Delta p_{T\ell\ell} = |p_{T\ell_1} - p_{T\ell_2}| \quad (10)$$

have been used [18, 23] to distinguish the transverse W background from the longitudinal W signal. The distributions in these variables for the $W^+W^- \rightarrow \bar{\ell}\nu\ell\nu$ events are shown in Fig. 11 at the SSC energy. Because of the success of our jet cuts, additional cuts on these variables would not improve the background suppression appreciably. However, these distributions of the $m_H = 1$ TeV signal have a shape different from that of the transverse W contributions and the QCD backgrounds and can hence serve as another independent verification that the backgrounds have indeed been suppressed.

Quantitative effects of cuts on $\phi_{\ell\ell}$ and $\Delta p_{T\ell\ell}$ are given in part (b) of Table II. A $\phi_{\ell\ell} > 140^\circ$ or $\Delta p_{T\ell\ell} > 300$ GeV cut increases the significance S/\sqrt{B} by 1 or 2σ , with a 15% reduction in the signal. It seems likely that we can obtain an overall significance level above 10σ by fully exploring the characteristics of the lepton distributions.

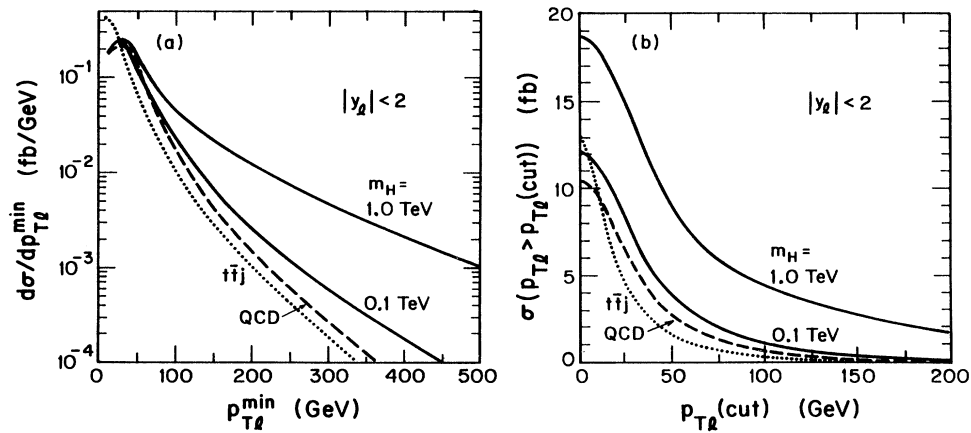


FIG. 10. (a) Transverse-momentum distributions $d\sigma/dp_{T\ell}^{\min}$ and (b) integrated cross section versus $p_{T\ell}(\text{cut})$, of the W decay leptons with $|y_\ell| < 2$ for the $t\bar{t}j$, QCD WWj , and electroweak $qqWW$ ($m_H = 0.1$ TeV) backgrounds and the SM heavy-Higgs-boson signal for $m_H = 1$ TeV at the SSC. Acceptance criteria are given in Eqs. (8a) and (9).

TABLE II. SSC cross section in fb for modified acceptance cuts on the final-state leptons. The forward-jet tagging and central-jet vetoing requirements of Eqs. (8a) and (9) are imposed everywhere. The significance S/\sqrt{B} is for $m_H = 1$ TeV, $m_t = 140$ GeV, and an integrated luminosity of 10 fb^{-1} .

	m_H (TeV)			QCD	$t\bar{t}j$	S/\sqrt{B}
	1.0	0.6	0.1			
(a) Relaxed $p_{T\ell}$ cut						
$p_{T\ell}$ cut						
0	19	19	12	11	14	39
60	7.0	8.6	3.2	1.9	1.2	4.5
100	4.6	4.6	1.0	0.60	0.42	1.6
(b) Added $\phi_{\ell\ell}$ or $\Delta p_{T\ell\ell}$ cut ($p_{T\ell} > 100 \text{ GeV}$ and $ y_\ell < 2$)						
$\phi_{\ell\ell} > 140^\circ$	3.9	3.5	0.58	0.26	0.33	1.3
$\Delta p_{T\ell\ell} > 300 \text{ GeV}$	3.6	3.1	0.59	0.27	0.26	0.96

The invariant-mass distributions of the decay leptons from W^+W^- are shown in Fig. 12. The $\ell^+\ell^-$ invariant-mass distribution of the $m_H = 1$ TeV signal has a broad peak at about $m_H/2$ while the electroweak and QCD backgrounds fall with increasing $m_{\ell\ell}$ above the effective kinematic threshold set by the $p_{T\ell} > 100 \text{ GeV}$ cut. Another useful variable is the cluster transverse mass of the $W^+W^- \rightarrow \bar{\ell}\nu\ell\bar{\nu}$ system, defined by [24]

$$M_T^2(\ell\ell, \not{p}_T) = \left(\sqrt{M_{\ell\ell}^2 + p_{T\ell\ell}^2} + |\not{p}_T| \right)^2 - (p_{T\ell\ell} + |\not{p}_T|)^2. \quad (11)$$

After imposing a missing transverse momentum acceptance cut of $\not{p}_T > 75 \text{ GeV}$, we obtain the cluster transverse mass distributions in Fig. 13. The M_T distribution also shows a broad peak for the signal with its maximum near $\frac{3}{4}m_H$.

The dependence of the peak position on the Higgs-boson mass is displayed in Fig. 14, where the $\ell^+\ell^-$

invariant-mass and the cluster transverse-mass distributions are compared for $m_H = 0.6 \text{ TeV}$, 0.8 TeV , and 1.0 TeV . These distributions for the $W^+W^- \rightarrow \bar{\ell}\nu\ell\bar{\nu}$ decay channel will provide useful information on the heavy-Higgs-boson mass.

V. CONCLUSIONS

We have studied the possibility of isolating the signal of a heavy Higgs boson in the process $qq \rightarrow W^+W^-qq$ with both W bosons decaying to $e\nu$ or $\mu\nu$ final states. This channel has a sizable event rate at hadron supercolliders but there are potentially severe backgrounds from QCD production of W^+W^-j and from $t\bar{t}j$ production where both top quarks decay into real W 's. Our results may be summarized as follows.

(a) The requirement of a single energetic forward jet having $3 < |\eta_j(\text{tag})| < 5$ and $E_j(\text{tag}) > 3 \text{ TeV}$ for the SSC and $E_j(\text{tag}) > 2 \text{ TeV}$ for the LHC largely eliminates the W^+W^-j background and reduces the $t\bar{t}j$ background

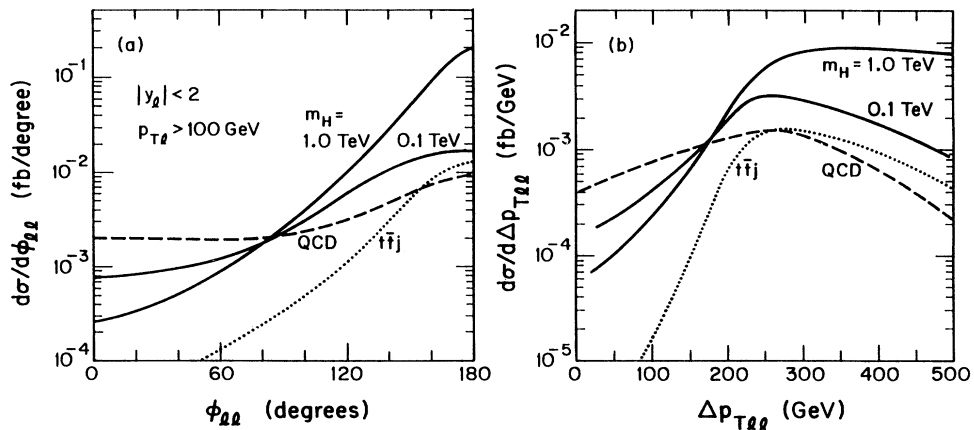


FIG. 11. Distribution in (a) the opening angle and (b) momentum difference of the leptons in the transverse plane at the SSC. Acceptance criteria are the same as in Fig. 7.

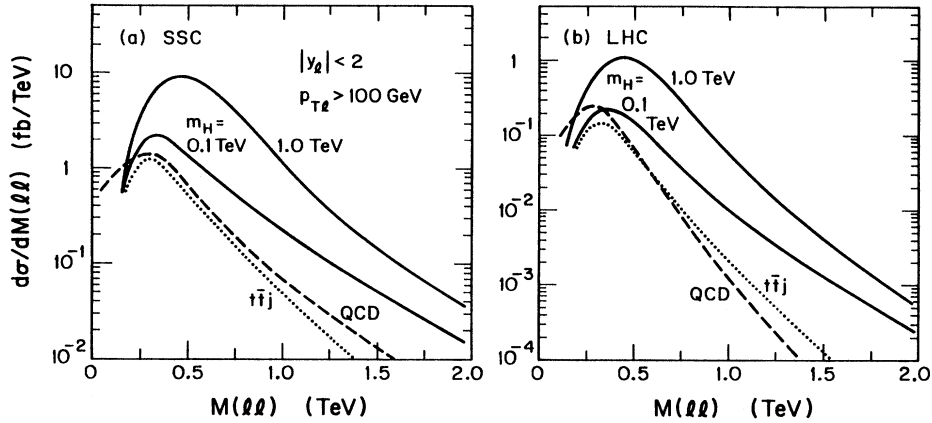


FIG. 12. Lepton pair invariant-mass distribution for the Higgs-boson signal ($m_H = 1$ TeV), the electroweak $qqWW$ background ($m_H = 0.1$ TeV), the QCD WWj background, and the $t\bar{t}j$ background at (a) the SSC and (b) the LHC. Acceptance criteria are the same as in Fig. 7.

to a level comparable to the heavy-Higgs-boson signal.

(b) The further imposition of a veto on jets in the central region, having $p_{Tj}(\text{veto}) > 60$ GeV and $|\eta_j(\text{veto})| < 3$, reduces the $t\bar{t}j$ background by another order of magnitude.

(c) The surviving heavy-Higgs-boson signal rate for $m_H = 1$ TeV is 36 events per nominal SSC year with an integrated luminosity of 10 fb^{-1} . The remaining backgrounds are estimated to be 10 electroweak $qqWW$ background events (calculated as the $m_H = 0.1$ TeV cross section), 6 WWj events and 4 $t\bar{t}j$ events. At the LHC with the same luminosity, the corresponding numbers for the signal and backgrounds are about an order of magni-

tude smaller with a slightly smaller signal-to-background ratio.

(d) We find that $H \rightarrow W^+W^- \rightarrow \bar{\ell}\nu\ell\nu$ is a viable discovery channel for the heavy Higgs boson, with event rates exceeding the $H \rightarrow ZZ \rightarrow 4\ell$ signal even in the jet-inclusive mode of the latter, which suffers from large QCD background contributions.

(e) Measurement of both $H \rightarrow WW$ and $H \rightarrow ZZ$ signals is important to verify the relative factor of 2 in the partial widths predicted by the electroweak SU(2) symmetry.

(f) The kinematical distributions of the final-state leptons and jets for a heavy-Higgs-boson signal, after

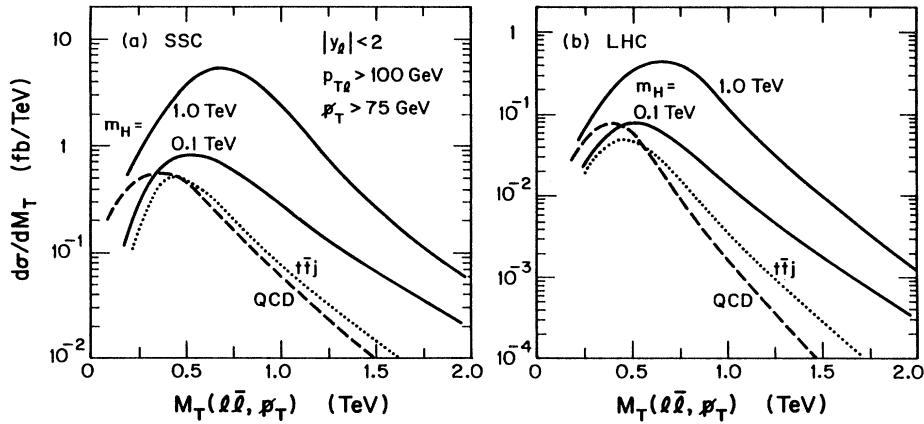


FIG. 13. Cluster transverse-mass distribution in W^+W^- events for the Higgs-boson signal ($m_H = 1$ TeV), and the $t\bar{t}j$, the QCD WWj , and the electroweak $qqWW$ ($m_H = 0.1$ TeV) backgrounds at (a) the SSC and (b) the LHC. Acceptance criteria are the same as in Fig. 7; in addition a missing-transverse-momentum cut of $\cancel{p}_T > 75$ GeV is imposed.

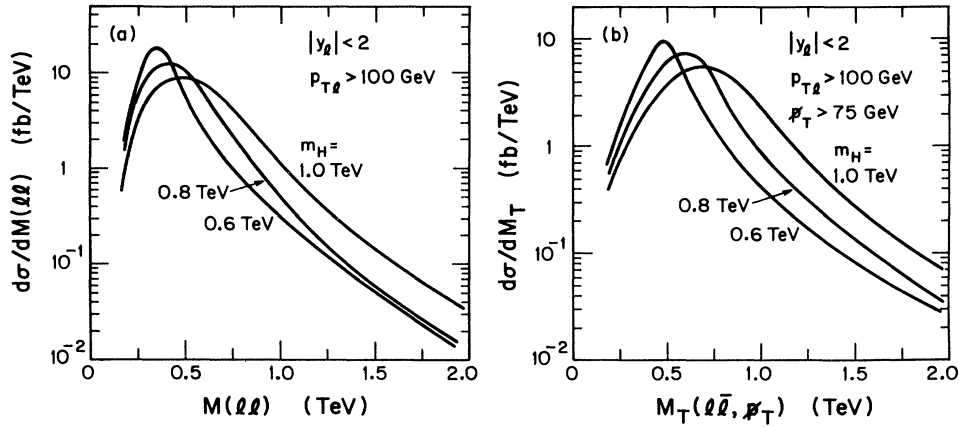


FIG. 14. Mass distributions (a) $M(\ell\ell)$ and (b) $M_T(\ell\bar{\ell}, \not{p}_T)$ at the SSC energy from the $qq \rightarrow qqW^+W^-$ subprocess for $m_H = 0.6, 0.8,$ and 1.0 TeV. Acceptance criteria are the same as in Fig. 7.

forward-jet tagging and central-jet vetoing, have distinguishing characteristics from that of electroweak transverse W -boson production; this allows positive identification of the heavy-Higgs-boson signal.

(g) The default value for the top-quark mass in our analysis was 140 GeV, but we found that the above conclusions are valid for $m_t > 100$ GeV.

(h) Our jet-tagging and jet-vetoing conditions are sim-

ilarly useful in sorting out the signal for a lighter Higgs boson. For example, for $m_H = 0.6$ TeV the same acceptance cuts also give 36 Higgs-boson signal events.

(i) If nature has chosen some strong electroweak-symmetry-breaking mechanism other than a heavy Higgs boson, the jet-tag and jet-veto techniques developed in this paper will be useful in separating the $W_L^+W_L^-$ scattering signal from the $t\bar{t}j$, QCD WWj , and electroweak

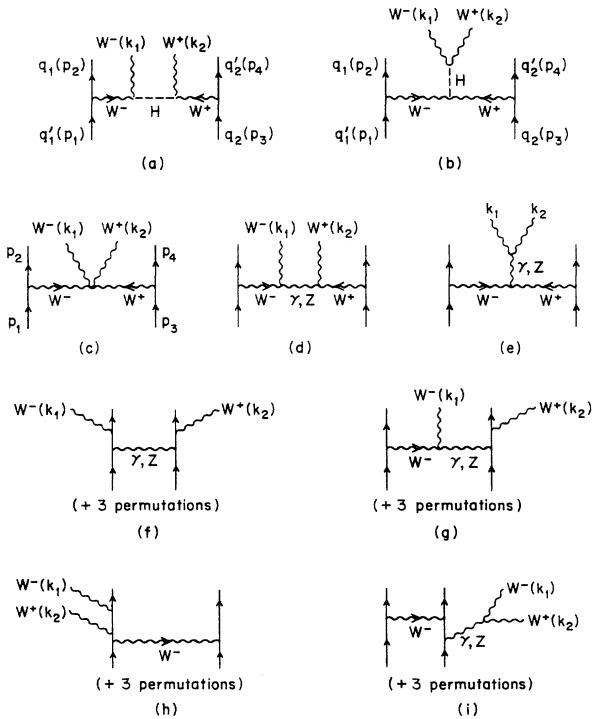


FIG. 15. Feynman graphs for the electroweak $qq \rightarrow qqW^+W^-$ process at order α^4 involving charged-current exchange.

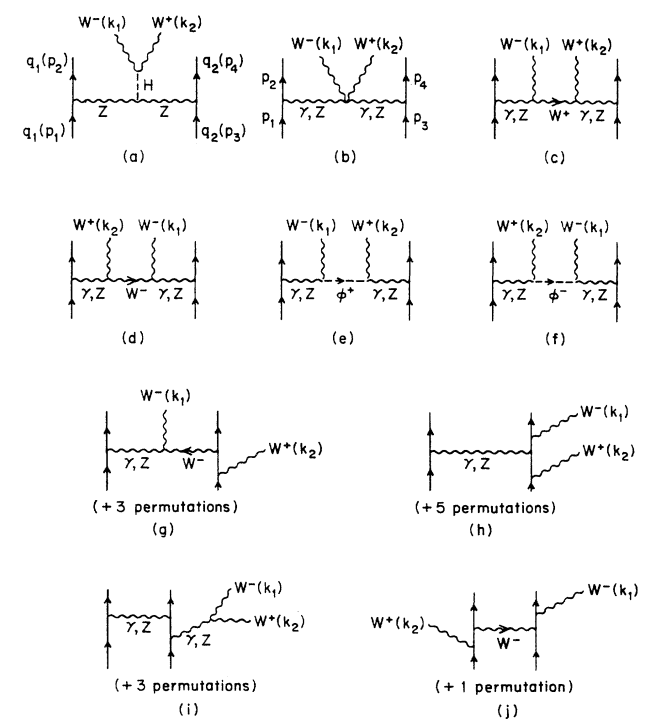


FIG. 16. Feynman graphs for the electroweak $qq \rightarrow qqW^+W^-$ process at order α^4 involving neutral-current exchange.

$qqWW$ backgrounds.

In summary, our procedures give the first definitive isolation of the heavy-Higgs-boson signal in the $H \rightarrow W^+W^- \rightarrow \bar{\ell}\nu\ell\bar{\nu}$ channel.

ACKNOWLEDGMENTS

We thank U. Baur and J. Ohnemus for helpful discussions. This research was supported in part by the University of Wisconsin Research Committee with funds granted by the Wisconsin Alumni Research Foundation, in part by the U.S. Department of Energy under Contract No. DE-AC02-76ER00881, and in part by the Texas National Laboratory Research Commission under Grant No. RGFY9173.

APPENDIX

This appendix gives all the formulas used in the calculation of the SM electroweak subprocess

$$qq \rightarrow qqW^+W^- . \quad (\text{A1})$$

There are two sets of Feynman graphs corresponding to charged-current exchange and neutral-current exchange. Here we give the helicity-amplitude expressions for the scattering matrix elements. For notation and conventions, we refer the reader to Refs. [16, 17]. All fermion masses are neglected. For diagrams of Fig. 15, which involve charged-current exchange, the flavors of the external quarks are $q = u, c$ and $q' = s, d$. The amplitudes are given by

$$i\mathcal{M}^{(a)} = -g^2 M_W^2 g_{\sigma_1}^W g_{\sigma_3}^W F_0 D^W(p_1 - p_2) D^W(p_3 - p_4) D^H(p_1 - p_2 - k_1) \times \langle p_2 | [f(k_1)]_{\sigma_1} | p_1 \rangle \langle p_4 | [f(k_2)]_{\sigma_3} | p_3 \rangle , \quad (\text{A2})$$

$$i\mathcal{M}^{(b)} = -g^2 M_W^2 g_{\sigma_1}^W g_{\sigma_3}^W F_0 D^W(p_1 - p_2) D^W(p_3 - p_4) D^H(k_1 + k_2) \epsilon(k_1) \cdot \epsilon(k_2) \times \langle p_2 | (\sigma^\mu)_{\sigma_1} | p_1 \rangle \langle p_4 | (\sigma_\mu)_{\sigma_3} | p_3 \rangle , \quad (\text{A3})$$

$$i\mathcal{M}^{(c)} = g^2 g_{\sigma_1}^W g_{\sigma_3}^W F_0 D^W(p_1 - p_2) D^W(p_3 - p_4) \times \{ 2 \langle p_4 | [f(k_1)]_{\sigma_3} | p_3 \rangle \langle p_2 | [f(k_2)]_{\sigma_1} | p_1 \rangle - \langle p_4 | [f(k_2)]_{\sigma_3} | p_3 \rangle \langle p_2 | [f(k_1)]_{\sigma_1} | p_1 \rangle - \epsilon(k_1) \cdot \epsilon(k_2) \langle p_2 | (\sigma^\mu)_{\sigma_1} | p_1 \rangle \langle p_4 | (\sigma_\mu)_{\sigma_3} | p_3 \rangle \} , \quad (\text{A4})$$

$$i\mathcal{M}^{(d)} = \sum_{V=\gamma, Z} g_{\sigma_1}^W g_{\sigma_3}^W F_0 (g_{VWW})^2 D^W(p_1 - p_2) D^W(p_3 - p_4) D^V(p_1 - p_2 - k_1) P_V^{\mu\nu}(p_1 - p_2 - k_1) \times \Gamma_\mu(p_1 - p_2, -k_1; \langle p_2 | (\sigma)_{\sigma_1} | p_1 \rangle, \epsilon(k_1)) \Gamma_\nu(-k_2, p_3 - p_4; \epsilon(k_2), \langle p_4 | (\sigma)_{\sigma_3} | p_3 \rangle) ,$$

where

$$g_{VWW} = \begin{cases} e \cot \theta_W & \text{if } V = Z , \\ e & \text{if } V = \gamma , \end{cases} \quad (\text{A5})$$

$$i\mathcal{M}^{(e)} = \sum_{V=\gamma, Z} g_{\sigma_1}^W g_{\sigma_3}^W F_0 (g_{VWW})^2 D^W(p_1 - p_2) D^W(p_3 - p_4) D^V(k_1 + k_2) \times \Gamma^\mu(p_1 - p_2, p_3 - p_4; \langle p_2 | (\sigma)_{\sigma_1} | p_1 \rangle, \langle p_4 | (\sigma)_{\sigma_3} | p_3 \rangle) \Gamma_\mu(k_1, k_2; \epsilon(k_1), \epsilon(k_2)) , \quad (\text{A6})$$

$$i\mathcal{M}^{(f)} = \sum_{V=\gamma, Z} g_{\sigma_1}^W g_{\sigma_3}^W F_0 D^V(p_1 - p_2 - k_1) P_V^{\mu\nu}(p_1 - p_2 - k_1) \times [g_{\sigma_1}^V(q'_1) \langle p_2 k_1 | (\sigma_\mu)_{\sigma_1} | p_1 \rangle + g_{\sigma_1}^V(q_1) \langle p_2 | (\sigma_\mu)_{\sigma_1} | k_1 p_1 \rangle] \times [g_{\sigma_3}^V(q_2) \langle p_4 k_2 | (\sigma_\nu)_{\sigma_3} | p_3 \rangle + g_{\sigma_3}^V(q'_2) \langle p_4 | (\sigma_\nu)_{\sigma_3} | k_2 p_3 \rangle] , \quad (\text{A7})$$

$$i\mathcal{M}^{(g)} = \sum_{V=\gamma, Z} [-g_{\sigma_1}^W g_{\sigma_3}^W F_0 g_{VWW} D^V(p_1 - p_2 - k_1) P_V^{\mu\nu}(p_1 - p_2 - k_1) \times \{ D^W(p_1 - p_2) \Gamma_\mu(p_1 - p_2, -k_1; \langle p_2 | (\sigma)_{\sigma_1} | p_1 \rangle, \epsilon(k_1)) \times [g_{\sigma_3}^V(q_2) \langle p_4 k_2 | (\sigma_\nu)_{\sigma_3} | p_3 \rangle + g_{\sigma_3}^V(q'_2) \langle p_4 | (\sigma_\nu)_{\sigma_3} | k_2 p_3 \rangle] + D^W(p_3 - p_4) \Gamma_\mu(-k_2, p_3 - p_4; \epsilon(k_2), \langle p_4 | (\sigma)_{\sigma_3} | p_3 \rangle) \times [g_{\sigma_1}^V(q'_1) \langle p_2 k_1 | (\sigma_\nu)_{\sigma_1} | p_1 \rangle + g_{\sigma_1}^V(q_1) \langle p_2 | (\sigma_\nu)_{\sigma_1} | k_1 p_1 \rangle] \}] , \quad (\text{A8})$$

$$\begin{aligned}
i\mathcal{M}^{(h)} = & (g_{\sigma_1}^W)^3 g_{\sigma_3}^W F_0 D^W(p_3 - p_4) \langle p_4 | (\sigma^\mu)_{\sigma_3} | p_3 \rangle [\langle p_2 k_1 k_2 | (\sigma_\mu)_{\sigma_1} | p_1 \rangle + \langle p_2 | (\sigma_\mu)_{\sigma_1} | k_2 k_1 p_1 \rangle] \\
& + (g_{\sigma_1}^W) (g_{\sigma_3}^W)^3 F_0 D^W(p_1 - p_2) \langle p_2 | (\sigma^\mu)_{\sigma_1} | p_1 \rangle [\langle p_4 k_2 k_1 | (\sigma_\mu)_{\sigma_3} | p_3 \rangle + \langle p_4 | (\sigma_\mu)_{\sigma_3} | k_1 k_2 p_3 \rangle],
\end{aligned} \tag{A9}$$

$$\begin{aligned}
i\mathcal{M}^{(i)} = & \sum_{V=\gamma, Z} (- g_{VWW} g_{\sigma_1}^W g_{\sigma_3}^W F_0 \\
& \times \{ D^W(p_3 - p_4) D^V(k_1 + k_2) [g_{\sigma_1}^V(q'_1) \langle p_2 | (\sigma^\mu)_{\sigma_1} | k_1 + k_2, p_1 \rangle \langle p_4 | (\sigma_\mu)_{\sigma_3} | p_3 \rangle \\
& \quad + g_{\sigma_1}^V(q_1) \langle p_2, k_1 + k_2 | (\sigma^\mu)_{\sigma_1} | p_1 \rangle \langle p_4 | (\sigma_\mu)_{\sigma_3} | p_3 \rangle] \\
& + D^W(p_1 - p_2) D^V(k_1 + k_2) [g_{\sigma_3}^V(q'_2) \langle p_4, k_1 + k_2 | (\sigma^\mu)_{\sigma_3} | p_3 \rangle \langle p_2 | (\sigma_\mu)_{\sigma_1} | p_1 \rangle \\
& \quad + g_{\sigma_3}^V(q_2) \langle p_4 | (\sigma^\mu)_{\sigma_3} | k_1 + k_2, p_3 \rangle \langle p_2 | (\sigma_\mu)_{\sigma_1} | p_1 \rangle] \}),
\end{aligned}$$

where

$$\begin{aligned}
\langle p_2, k_1 + k_2 | & = \chi_{\sigma_1}^\dagger(\bar{p}_2) [\mathcal{F}(k_1, k_2; \epsilon(k_1), \epsilon(k_2))]_{\sigma_1} \frac{(\not{p}_2 + \not{k}_1 + \not{k}_2)_{-\sigma_1}}{(p_2 + k_1 + k_2)^2}, \\
|k_1 + k_2, p_1 \rangle & = \frac{(\not{p}_1 - \not{k}_1 - \not{k}_2)_{-\sigma_1}}{(p_1 - k_1 - k_2)^2} [\mathcal{F}(k_1, k_2; \epsilon(k_1), \epsilon(k_2))]_{\sigma_1} \chi_{\sigma_1}(\bar{p}_1).
\end{aligned} \tag{A10}$$

The neutral-current-exchange subprocesses are shown in Fig. 16. In the case that two W 's radiate from a single quark line, the order of W^+ , W^- attached to the quark line depends on the initial flavors. In diagrams (g), (h), and (j) special care is needed; here the Kronecker δ is used to denote the flavor of initial quarks (e.g., $\delta_{q_1, d}$ means q_1 is a d quark or an s quark). The individual Feynman diagrams contribute as follows (q_1 and q_2 can now be any flavors):

$$\begin{aligned}
i\mathcal{M}^{(a)} = & - \frac{g^2}{1 - x_W} g_{\sigma_1}^Z(q_1) g_{\sigma_3}^Z(q_2) M_W^2 D^Z(p_1 - p_2) D^Z(p_3 - p_4) D^H(k_1 + k_2) F_0 \\
& \times \epsilon(k_1) \cdot \epsilon(k_2) \langle p_4 | (\sigma^\mu)_{\sigma_3} | p_3 \rangle \langle p_2 | (\sigma_\mu)_{\sigma_1} | p_1 \rangle,
\end{aligned} \tag{A11}$$

$$\begin{aligned}
i\mathcal{M}^{(b)} = & \sum_{\substack{V_1=\gamma, Z \\ V_2=\gamma, Z}} (- g_{\sigma_1}^{V_1}(q_1) g_{\sigma_3}^{V_2}(q_2) g_{V_1WW} g_{V_2WW} F_0 D^{V_1}(p_1 - p_2) D^{V_2}(p_3 - p_4) \\
& \times \{ 2 \langle p_2 | (\sigma^\mu)_{\sigma_1} | p_1 \rangle \langle p_4 | (\sigma_\mu)_{\sigma_3} | p_3 \rangle \epsilon(k_1) \cdot \epsilon(k_2) \\
& \quad - \langle p_2 | [\mathcal{f}(k_1)]_{\sigma_1} | p_1 \rangle \langle p_4 | [\mathcal{f}(k_2)]_{\sigma_3} | p_3 \rangle - \langle p_2 | [\mathcal{f}(k_2)]_{\sigma_1} | p_1 \rangle \langle p_4 | [\mathcal{f}(k_1)]_{\sigma_3} | p_3 \rangle \}),
\end{aligned} \tag{A12}$$

$$\begin{aligned}
i\mathcal{M}^{(c)} = & \sum_{\substack{V_1=\gamma, Z \\ V_2=\gamma, Z}} g_{V_1WW} g_{V_2WW} g_{\sigma_1}^{V_1}(q_1) g_{\sigma_3}^{V_2}(q_2) D^{V_1}(p_1 - p_2) D^{V_2}(p_3 - p_4) P_W^{\mu\nu}(p_1 - p_2 - k_1) \\
& \times \Gamma_\mu(-k_1, p_1 - p_2; \epsilon(k_1), \langle p_2 | (\sigma)_{\sigma_1} | p_1 \rangle) \Gamma_\nu(p_3 - p_4, -k_2; \langle p_4 | (\sigma)_{\sigma_3} | p_3 \rangle, \epsilon(k_2)),
\end{aligned} \tag{A13}$$

$$\begin{aligned}
i\mathcal{M}^{(d)} = & \sum_{\substack{V_1=\gamma, Z \\ V_2=\gamma, Z}} g_{V_1WW} g_{V_2WW} g_{\sigma_1}^{V_1}(q_1) g_{\sigma_3}^{V_2}(q_2) D^{V_1}(p_1 - p_2) D^{V_2}(p_3 - p_4) P_W^{\mu\nu}(p_1 - p_2 - k_2) \\
& \times \Gamma_\mu(p_1 - p_2, -k_2; \langle p_2 | (\sigma)_{\sigma_1} | p_1 \rangle, \epsilon(k_2)) \Gamma_\nu(-k_1, p_3 - p_4; \epsilon(k_1), \langle p_4 | (\sigma)_{\sigma_3} | p_3 \rangle),
\end{aligned} \tag{A14}$$

$$\begin{aligned}
i\mathcal{M}^{(e)} = & \sum_{\substack{V_1=\gamma, Z \\ V_2=\gamma, Z}} g_{V_1WW} g_{V_2WW} M_W^2 g_{\sigma_1}^{V_1}(q_1) g_{\sigma_3}^{V_2}(q_2) D^{V_1}(p_1 - p_2) D^{V_2}(p_3 - p_4) F_0 \\
& \times \frac{\xi}{\xi(p_1 - p_2 - k_1)^2 - M_W^2} \langle p_2 | [\mathcal{f}(k_1)]_{\sigma_1} | p_1 \rangle \langle p_4 | [\mathcal{f}(k_2)]_{\sigma_3} | p_3 \rangle \\
& \times \begin{cases} -\tan^4 \theta_W & \text{if } V_1 = V_2 = Z, \\ -1 & \text{if } V_1 = V_2 = \gamma, \\ \tan^2 \theta_W & \text{otherwise,} \end{cases}
\end{aligned} \tag{A15}$$

$$i\mathcal{M}^{(f)} = i\mathcal{M}^{(e)} \text{ with } (k_1 \leftrightarrow k_2), \tag{A16}$$

$$\begin{aligned}
i\mathcal{M}^{(g)} = & \sum_{V=\gamma,Z} [-g_{VWW}(g_{\sigma_3}^W)^2 g_{\sigma_1}^V(q_1) F_0 D^V(p_1 - p_2) \\
& \times \{D^W(p_1 - p_2 - k_1) P_W^{\mu\nu}(p_1 - p_2 - k_1) \Gamma_\mu(-k_1, p_1 - p_2; \epsilon(k_1), \langle p_2 | (\sigma)_{\sigma_1} | p_1 \rangle) \\
& \times [\delta_{q_2,d} \langle p_4 k_2 | (\sigma_\nu)_{\sigma_3} | p_3 \rangle + \delta_{q_2,u} \langle p_4 | (\sigma_\nu)_{\sigma_3} | k_2 p_3 \rangle] \\
& + D^W(p_1 - p_2 - k_2) P_W^{\mu\nu}(p_1 - p_2 - k_2) \Gamma_\mu(p_1 - p_2, -k_2; \langle p_2 | (\sigma)_{\sigma_1} | p_1 \rangle, \epsilon(k_2)) \\
& \times [\delta_{q_2,d} \langle p_4 | (\sigma_\nu)_{\sigma_3} | k_1 p_3 \rangle + \delta_{q_2,u} \langle p_4 k_1 | (\sigma_\nu)_{\sigma_3} | p_3 \rangle]\}] \\
& + \sum_{V=\gamma,Z} [-g_{VWW}(g_{\sigma_1}^W)^2 g_{\sigma_3}^V(q_2) F_0 D^V(p_3 - p_4) \\
& \times \{D^W(p_1 - p_2 - k_2) P_W^{\mu\nu}(p_1 - p_2 - k_2) \Gamma_\mu(-k_1, p_3 - p_4; \epsilon(k_1), \langle p_4 | (\sigma)_{\sigma_3} | p_3 \rangle) \\
& \times (\delta_{q_1,u} \langle p_2 | (\sigma_\nu)_{\sigma_1} | k_2 p_1 \rangle + \delta_{q_1,d} \langle p_2 k_2 | (\sigma_\nu)_{\sigma_1} | p_1 \rangle) \\
& + D^W(p_1 - p_2 - k_1) P_W^{\mu\nu}(p_1 - p_2 - k_1) \Gamma_\mu(p_3 - p_4, -k_2; \langle p_4 | (\sigma)_{\sigma_3} | p_3 \rangle, \epsilon(k_2)) \\
& \times (\delta_{q_1,u} \langle p_2 k_1 | (\sigma_\nu)_{\sigma_1} | p_1 \rangle + \delta_{q_1,d} \langle p_2 | (\sigma_\nu)_{\sigma_1} | k_1 p_1 \rangle)\}] , \tag{A17}
\end{aligned}$$

$$\begin{aligned}
i\mathcal{M}^{(h)} = & \sum_{V=\gamma,Z} g_{\sigma_1}^V(q_1) (g_{\sigma_3}^W)^2 F_0 D^V(p_1 - p_2) \langle p_2 | (\sigma^\mu)_{\sigma_1} | p_1 \rangle \\
& \times \{ \delta_{q_2,u} [\langle p_4 k_1 | (\sigma_\mu)_{\sigma_3} | k_2 p_3 \rangle g_{\sigma_3}^V(q_2') + \langle p_4 | (\sigma_\mu)_{\sigma_3} | k_1 k_2 p_3 \rangle g_{\sigma_3}^V(q_2) \\
& + \langle p_4 k_1 k_2 | (\sigma_\mu)_{\sigma_3} | p_3 \rangle g_{\sigma_3}^V(q_2)] \\
& + \delta_{q_2,d} [\langle p_4 k_2 | (\sigma_\mu)_{\sigma_3} | k_1 p_3 \rangle g_{\sigma_3}^V(q_2') + \langle p_4 | (\sigma_\mu)_{\sigma_3} | k_2 k_1 p_3 \rangle g_{\sigma_3}^V(q_2) \\
& + \langle p_4 k_2 k_1 | (\sigma_\mu)_{\sigma_3} | p_3 \rangle g_{\sigma_3}^V(q_2)] \} \\
& + \sum_{V=\gamma,Z} g_{\sigma_3}^V(q_2) (g_{\sigma_1}^W)^2 F_0 D^V(p_3 - p_4) \langle p_4 | (\sigma^\mu)_{\sigma_3} | p_3 \rangle \\
& \times \{ \delta_{q_1,u} [\langle p_2 k_1 | (\sigma_\mu)_{\sigma_1} | k_2 p_1 \rangle g_{\sigma_1}^V(q_1') + \langle p_2 | (\sigma_\mu)_{\sigma_1} | k_1 k_2 p_1 \rangle g_{\sigma_1}^V(q_1) \\
& + \langle p_2 k_1 k_2 | (\sigma_\mu)_{\sigma_1} | p_1 \rangle g_{\sigma_1}^V(q_1)] \\
& + \delta_{q_1,d} [\langle p_2 k_2 | (\sigma_\mu)_{\sigma_1} | k_1 p_1 \rangle g_{\sigma_1}^V(q_1') + \langle p_2 | (\sigma_\mu)_{\sigma_1} | k_2 k_1 p_1 \rangle g_{\sigma_1}^V(q_1) \\
& + \langle p_2 k_2 k_1 | (\sigma_\mu)_{\sigma_1} | p_1 \rangle g_{\sigma_1}^V(q_1)] \} , \tag{A18}
\end{aligned}$$

$$\begin{aligned}
i\mathcal{M}^{(i)} = & \sum_{\substack{V_1=\gamma,Z \\ V_2=\gamma,Z}} \{-g_{V_1WW} g_{\sigma_1}^{V_1}(q_1) g_{\sigma_1}^{V_2}(q_1) g_{\sigma_3}^{V_2}(q_2) D^{V_1}(k_1 + k_2) D^{V_2}(p_3 - p_4) F_0 \\
& \times \langle p_4 | (\sigma^\mu)_{\sigma_3} | p_3 \rangle [\langle p_2 | (\sigma^\mu)_{\sigma_1} | k_1 + k_2, p_1 \rangle + \langle p_2, k_1 + k_2 | (\sigma^\mu)_{\sigma_1} | p_1 \rangle]\} \\
& + \sum_{\substack{V_1=\gamma,Z \\ V_2=\gamma,Z}} \{-g_{V_2WW} g_{\sigma_1}^{V_1}(q_1) g_{\sigma_3}^{V_1}(q_2) g_{\sigma_3}^{V_2}(q_2) D^{V_1}(p_1 - p_2) D^{V_2}(k_1 + k_2) F_0 \\
& \times \langle p_2 | (\sigma^\mu)_{\sigma_1} | p_1 \rangle [\langle p_4, k_1 + k_2 | (\sigma_\mu)_{\sigma_3} | p_3 \rangle + \langle p_4 | (\sigma_\mu)_{\sigma_3} | k_1 + k_2, p_3 \rangle]\} , \tag{A19}
\end{aligned}$$

$$\begin{aligned}
i\mathcal{M}^{(j)} = & (g_{\sigma_1}^W)^2 (g_{\sigma_3}^W)^2 F_0 \\
& \times \{ \delta_{q_1,u} \delta_{q_2,u} [D^W(p_1 - p_2 - k_2) P_W^{\mu\nu}(p_1 - p_2 - k_2) \langle p_2 | (\sigma_\mu)_{\sigma_1} | k_2 p_1 \rangle \langle p_4 k_1 | (\sigma_\nu)_{\sigma_3} | p_3 \rangle \\
& + D^W(p_1 - p_2 - k_1) P_W^{\mu\nu}(p_1 - p_2 - k_1) \langle p_2 k_1 | (\sigma_\mu)_{\sigma_1} | p_1 \rangle \langle p_4 | (\sigma_\nu)_{\sigma_3} | k_2 p_3 \rangle] \\
& + \delta_{q_1,u} \delta_{q_2,d} [D^W(p_1 - p_2 - k_2) P_W^{\mu\nu}(p_1 - p_2 - k_2) \langle p_2 | (\sigma_\mu)_{\sigma_1} | k_2 p_1 \rangle \langle p_4 | (\sigma_\nu)_{\sigma_3} | k_1 p_3 \rangle \\
& + D^W(p_1 - p_2 - k_1) P_W^{\mu\nu}(p_1 - p_2 - k_1) \langle p_2 k_1 | (\sigma_\mu)_{\sigma_1} | p_1 \rangle \langle p_4 k_2 | (\sigma_\nu)_{\sigma_3} | p_3 \rangle] \\
& + \delta_{q_1,d} \delta_{q_2,u} [D^W(p_1 - p_2 - k_2) P_W^{\mu\nu}(p_1 - p_2 - k_2) \langle p_2 k_2 | (\sigma_\mu)_{\sigma_1} | p_1 \rangle \langle p_4 k_1 | (\sigma_\nu)_{\sigma_3} | p_3 \rangle \\
& + D^W(p_1 - p_2 - k_1) P_W^{\mu\nu}(p_1 - p_2 - k_1) \langle p_2 | (\sigma_\mu)_{\sigma_1} | k_1 p_1 \rangle \langle p_4 | (\sigma_\nu)_{\sigma_3} | k_2 p_3 \rangle] \\
& + \delta_{q_1,d} \delta_{q_2,d} [D^W(p_1 - p_2 - k_2) P_W^{\mu\nu}(p_1 - p_2 - k_2) \langle p_2 k_2 | (\sigma_\mu)_{\sigma_1} | p_1 \rangle \langle p_4 | (\sigma_\nu)_{\sigma_3} | k_1 p_3 \rangle \\
& + D^W(p_1 - p_2 - k_1) P_W^{\mu\nu}(p_1 - p_2 - k_1) \langle p_2 | (\sigma_\mu)_{\sigma_1} | k_1 p_1 \rangle \langle p_4 k_2 | (\sigma_\nu)_{\sigma_3} | p_3 \rangle] \} . \tag{A20}
\end{aligned}$$

In both charged- and neutral-current subprocesses the complete matrix element must be antisymmetrized in (p_1, σ_1) (p_3, σ_3) or (p_2, σ_2) (p_4, σ_4) , when identical flavors occur on the two incoming or outgoing fermion lines.

To include the subsequent decays $W^\pm \rightarrow \ell^\pm \nu$, we replace

$$\epsilon^\mu(k_1) \rightarrow \frac{g}{\sqrt{2}} \sqrt{4\bar{\ell}^0 \bar{\nu}^0} D^W(\ell^- + \bar{\nu}) \delta_{\sigma_\nu \sigma_\ell} \langle \ell^- | (\sigma^\mu)_{\sigma_\nu} | \bar{\nu} \rangle, \quad (\text{A21})$$

$$\epsilon^\mu(k_2) \rightarrow \frac{g}{\sqrt{2}} \sqrt{4\bar{\ell}^0 \bar{\nu}^0} D^W(\ell^+ + \nu) \delta_{\sigma_\nu \sigma_\ell} \langle \nu | (\sigma^\mu)_{\sigma_\nu} | \ell^+ \rangle, \quad (\text{A22})$$

in the above expressions, and we use the narrow-width approximation.

-
- [1] J. F. Gunion, G. L. Kane, H. E. Haber, and S. Dawson, *The Higgs Hunter's Guide* (Addison-Wesley, Reading, MA, 1989); J. F. Gunion *et al.*, in *Research Directions for the Decade*, Proceedings of the Summer Study, Snowmass, Colorado, 1990 (Editions Frontieres, Gif-sur-Yvette, in press).
- [2] M. S. Chanowitz and M. K. Gaillard, Nucl. Phys. **B261**, 375 (1985); M. S. Chanowitz, Annu. Rev. Nucl. Part. Sci. **38**, 323 (1985); M. S. Chanowitz and M. Golden, Phys. Rev. Lett. **61**, 1053 (1988); **63**, 466(E) (1989); A. Dobado and M. J. Herrero, Phys. Lett. B **228**, 195 (1989); F. Donoghue and C. Ramirez, *ibid.* **234**, 361 (1990); A. Dobado, M. J. Herrero, and T. N. Truong, *ibid.* **235**, 129 (1990); D. Dicus and W. Repko, Phys. Rev. D **42**, 3660 (1990).
- [3] G. Kane and C. P. Yuan, Phys. Rev. D **40**, 2231 (1989).
- [4] V. Barger, K. Cheung, T. Han, and R. J. N. Phillips, Phys. Rev. D **42**, 3052 (1990).
- [5] S. D. Ellis, R. Kleiss, and W. J. Stirling, Phys. Lett. **154B**, 435 (1985); R. Kleiss and W. J. Stirling, Nucl. Phys. **B262**, 235 (1985); Phys. Lett. B **180**, 171 (1986); J. F. Gunion, Z. Kunszt, and M. Soldate, Phys. Lett. **163B**, 389 (1985); **168B**, 427(E) (1986); J. F. Gunion and M. Soldate, Phys. Rev. D **34**, 826(1986); R. K. Ellis and R. J. Gonsalves, in *Supercollider Physics*, Proceedings of the Topical Conference, Eugene, Oregon, 1985, edited by D. E. Soper (World Scientific, Singapore, 1986).
- [6] R. K. Ellis and J. C. Sexton, Nucl. Phys. **B282**, 642 (1987).
- [7] P. Nason, S. Dawson, and R. K. Ellis, Nucl. Phys. **B303**, 607 (1988); W. Beenakker *et al.*, Phys. Rev. D **40**, 54 (1989); Nucl. Phys. **B351**, 507 (1991).
- [8] H. Baer, V. Barger, and R. J. N. Phillips, Phys. Rev. D **39**, 2809 (1989); H. Baer, V. Barger, J. Ohnemus, and R. J. N. Phillips, *ibid.* **42**, 54 (1990); R. P. Kauffman and C. P. Yuan, *ibid.* **42**, 956 (1990); G. A. Ladinsky and C. P. Yuan, *ibid.* **43**, 789 (1991).
- [9] R. Kleiss and W. J. Stirling, Phys. Lett. B **200**, 193 (1988); D. Froideveaux, in *Proceedings of the ECFA Large Hadron Collider Workshop*, Aachen, Germany, 1990, edited by G. Jarlskog and D. Rein (CERN Report No. 90-10, Geneva, Switzerland, 1990), Vol. II, p. 444; M. H. Seymour, *ibid.*, p. 557; D. Froideveaux, talk given at the SSC Physics Symposium, Madison, Wisconsin, 1991 (unpublished).
- [10] U. Baur, E. W. N. Glover, and J. J. van der Bij, Nucl. Phys. **B318**, 106 (1989).
- [11] V. Barger, T. Han, J. Ohnemus, and D. Zeppenfeld, Phys. Rev. D **41**, 2782 (1990).
- [12] CDF Collaboration, F. Abe *et al.*, Phys. Rev. D **43**, 664 (1991).
- [13] E. W. N. Glover and J. J. van der Bij, Phys. Lett. B **219**, 488 (1989); C. Kao and D. A. Dicus, Phys. Rev. D **43**, 1555 (1991).
- [14] D. A. Dicus and R. Vega, Phys. Rev. Lett. **57**, 1110 (1986); Phys. Rev. D **37**, 2427 (1988); J. F. Gunion, J. Kalinowski, and A. Tofighi-Niaki, Phys. Rev. Lett. **57**, 2351 (1986).
- [15] U. Baur and E. W. N. Glover, Phys. Lett. B **252**, 683 (1990).
- [16] K. Hagiwara and D. Zeppenfeld, Nucl. Phys. **B274**, 1 (1986); **B313**, 560 (1989).
- [17] V. Barger, K. Cheung, T. Han, J. Ohnemus, and D. Zeppenfeld, Phys. Rev. D **44**, 1426 (1991).
- [18] M. S. Berger and M. S. Chanowitz, Phys. Lett. B **263**, 509 (1991).
- [19] P. N. Harriman, A. D. Martin, R. G. Roberts, and W. J. Stirling, Phys. Rev. D **42**, 798 (1990).
- [20] V. Barger and R. J. N. Phillips, Phys. Rev. Lett. **55**, 2752 (1985); H. Baer, V. Barger, H. Goldberg, and R. J. N. Phillips, Phys. Rev. D **37**, 3152 (1988).
- [21] V. Barger, J. Ohnemus, and R. J. N. Phillips, Int. J. Mod. Phys. A **4**, 617 (1989).
- [22] V. Barger, G. Bhattacharya, T. Han, and B. A. Kniehl, Phys. Rev. D **43**, 779 (1991).
- [23] D. A. Dicus, J. F. Gunion, and R. Vega, Phys. Lett. B **258**, 475 (1991).
- [24] V. Barger, A. D. Martin, and R. J. N. Phillips, Phys. Lett. **125B**, 339(1983); V. Barger, T. Han, and J. Ohnemus, Phys. Rev. D **37**, 1174 (1988).